Comparison of Different Methods of Abel Inversion Using Computer Simulated and Experimental Side-On Data

G. Pretzler, H. Jäger, T. Neger, H. Philipp, and J. Woisetschläger

Institut für Experimentalphysik, Technische Universität Graz, Graz, Austria

Z. Naturforsch. **47a**, 955–970 (1992); received April 23, 1992

A recently devised new method for numerical Abel inversion is compared with four other commonly used methods. One of them, the convolution method, is employed in computer tomography for reconstructing asymmetrical objects. It is investigated whether this method can be adapted for the case of radial symmetry.

As a first approach the comparison is performed by computer simulation. Special attention is given to the propagation of errors according to their origin. The result is a recipe for minimizing errors and for choosing the optimal method for reconstruction.

The second step is a comparison of experimentally obtained radial profiles with functions resulting from Abel inversion of measured side-on data. Thus it is shown that the concept developed by computer simulation can be applied in practice.

1. Introduction

The problem of reconstructing a two-dimensional distribution from measured projections, or line integrals, occurs in many different disciplines of science from microscopy to astrophysics, the best-known application being medical computer tomography. A special case of this reconstruction problem is the Abel transformation which has to be used in the study of radially symmetrical objects (e.g. side-on observation of a plasma column), when an unknown function $f(r)$ (see Fig. 1.1) cannot be measured directly but only by integrating it along straight line paths, thus producing the projection $h(y)$. The relation between these two functions is given by the forward Abel transformation

$$h(y) = 2 \int_y^R f(r) \frac{r}{\sqrt{r^2 - y^2}} \, \mathrm{d}r \,. \tag{1.1}$$

The reconstruction of the unknown function $f(r)$ from the measured data $h(y)$ can be done analytically by means of the inverse Abel transformation [1]

$$f(r) = -\frac{1}{\pi} \int_y^R \frac{\mathrm{d}h(y)}{\mathrm{d}y} \cdot \frac{\mathrm{d}y}{\sqrt{y^2 - r^2}} \,. \tag{1.2}$$

In practice, the projection $h(y)$ is not given analytically but in the form of a certain number of measured data points. Thus both the differentiation and the integration in (1.2) cannot be performed directly. Very many numerical methods have been developed and used for performing these calculations e.g. [2–11]. In Sect. 2 of this paper we briefly describe some of these techniques, including the *convolution method* which is normally used for asymmetrical geometry. In Sect. 3 we compare these methods using computer simulation. Special interest is given to the error propagation caused by each reconstruction technique. For studying the practical relevance of these results we performed the experiment described in Sect. 4, which allows independent measurement of the radially symmetrical function $f(r)$ and the projection data $h(y)$. The latter

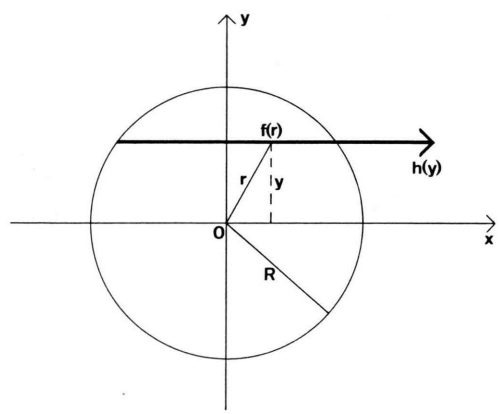

Fig. 1.1. *Situation in a plane perpendicular to the axis of symmetry:* The radially symmetrical distribution $f(r)$ cannot be measured directly but only through the integral $h(y)$ in the x-direction.

Reprint requests to Prof. Dr. H. Jäger, Institut für Experimentalphysik, Technische Universität Graz, Petersgasse 16, A-8010 Graz, Österreich.

0932-0784 / 92 / 0900-0955 $ 01.30/0. – Please order a reprint rather than making your own copy.

are reconstructed, the results being compared with the former. Thus we have a criterion for the reconstruction quality and so we can check the practical usability of the concepts developed by computer simulation.

2. Methods to be Compared

2.1. Survey

The oldest methods for numerically inverting the Abel equation (1.1) transform the measured data linearly into the unknown function using tabulated matrices. These matrices are calculated by discretizing either (1.1) or (1.2).

When more powerful computers became available, more sophisticated and complicated inversion techniques could be employed. Many methods are based on interpolation – either between the measured points of the distribution $h(y)$ or between the resulting points of the unknown function $f(r)$. In this paper from now on these methods will be referred to as *h-interpolation* and *f-interpolation*, respectively.

As an example for techniques developed recently we will also employ the so-called Fourier method. Here both a Fourier and an Abel transformation of the unknown function are performed, the Fourier coefficients being calculated from the measured data.

In the case of total asymmetry, equations different from (1.1) and (1.2) describe the situation, and therefore more complicated reconstruction procedures known as *computer tomography* must be used. Here such methods will be adapted for radially symmetrical geometry.

2.2. Matrix Method

There are many different ways of calculating matrices which connect the measured function $h(y)$ with the unknown distribution $f(r)$ by discretizing (1.1) or (1.2), see e.g. [2–4]. We used a method suggested in [5]. It is presumed that the value of the function $f(r)$ is constant in each of N rings around the symmetry axis:

$$f(r) = f_k = \text{const}, \quad \forall R_{k-1} > r \geq R_k \qquad (k = 1, \ldots, N).$$

Then by simple geometrical considerations one obtains N different values h_k of the projection $h(y)$:

$$h_k = \sum_{i=1}^{k} \underbrace{2 \cdot (\sqrt{R_{i-1}^2 - R_k^2} - \sqrt{R_i^2 - R_k^2})}_{a_{ik}} f_i . \qquad (2.1)$$

The matrix a_{ik} calculated from (2.1) is triangular and can therefore easily be inverted to obtain the values f_k out of the measured data points h_k.

2.3. h-Interpolation

Several authors (e.g. [6–8]) try to smooth or to interpolate the measured function $h(y)$ by means of simple functions which allow the differentiation and the integration in (1.2) to be performed analytically. We employed a method proposed in [9] using cubic spline interpolation of the measured data. Each two adjacent data points are connected by a polynomial of the third degree which must have the same first and second derivative as the polynomial for the next interval at the connecting point. Hence we have four conditions for each of the polynomials, and therefore we can calculate the four coefficients by solving a linear equation system. Now the measured function $h(y)$ (N measured points) is represented by $(N-1)$ polynomials:

$$h(y) = P_k(y) = \sum_{j=0}^{3} c_{j,k}\, y^j, \quad \begin{matrix} \forall y:\ y_k \leq y \leq y_{k+1} \\ (k = 0, \ldots, (N-2)) \end{matrix}, \qquad (2.2)$$

which is derived analytically and inserted into (1.2)

$$f(R_i) = -\frac{1}{\pi} \sum_{n=1}^{N-2} \int_{R_n}^{R_{n+1}} \sum_{j=0}^{2} a_{j,n}\, y^i \cdot \frac{1}{\sqrt{y^2 - R_i^2}}\, \mathrm{d}y$$

$$= -\frac{1}{\pi} \sum_{n=i}^{N-2} \sum_{j=0}^{2} a_{j,n} \cdot \underbrace{\int_{R_n}^{R_{n+1}} \frac{y^j}{\sqrt{y^2 - R_i^2}}\, \mathrm{d}y}_{I_j} . \qquad (2.3)$$

The integrals I_j can be solved analytically, thus yielding the resulting function $f(r)$ at N different discrete points $r = R_i$.

2.4. f-Interpolation

In contrast to Sect. 2.3 we also tried to interpolate the resulting distribution $f(r)$ and not the measured projection $h(y)$. We found that polynomials of the third degree can be employed:

$$f(r) = P_i(r) = A_i + B_i r + C_i r^2 + D_i r^3, \qquad (2.4)$$

$$R_i \geq r \geq R_{i+1}, \quad 0 \leq i < M < N .$$

M is the number of polynomials, N is the number of measured points. The unknown coefficients A_i, B_i, C_i,

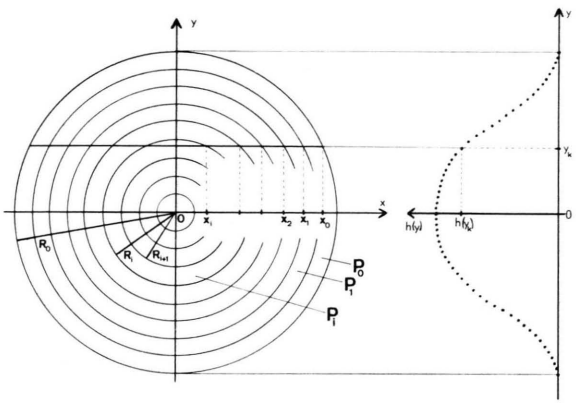

Fig. 2.1. *Geometry for polynomial interpolation:* the circular test zone is divided into rings. In each of them a polynomial $P_i(r)$ describes the distribution $f(r)$. Any measured point $h(y_k)$ lies on a beam intersecting several different rings.

D_i are calculated in the following way: Each polynomial $P_i(r)$ is assumed to have the same value as the neighbouring polynomials at four points, namely at the limiting points ($r = R_i$ and R_{i+1}) and at the limiting points of the two neighbouring polynomials ($r = R_{i-1}$ and R_{i+2}).

The calculation of the polynomials starts from the periphery of the reconstructing area (P_0) and is continued gradually to the centre (P_{M-1}). Hence, when calculating the coefficients of the polynomial (P_i), the polynomials $P_0 \ldots P_{i-1}$ are already known and consequently also the values of the unknown polynomial $P_i(r)$ are known at the points $r = R_{i-1}$ and R_i (and even at the point $r = R_{i+1}$, but we do not use this information). This gives two equations for the four coefficients, and only two of them (e.g. A_i and B_i) remain independent. Considering (cf. Fig. 2.1) that the integration path for an arbitrary measured point y_k intersects zones of different polynomials, and transforming (1.1) we get

$$h(y_k) = 2 \sum_{j=0}^{i-1} \int_{x_{j+1}}^{x_j} P_j(\sqrt{x^2 + y_k^2})\, \mathrm{d}x + 2 \int_0^{x_i} P_i(\sqrt{x^2 + y_k^2}, A_i, B_i)\, \mathrm{d}x = K(y_k) + L(y_k, A_i, B_i), \tag{2.5}$$

i = number of innermost intersected zone (see Fig. 2.1),
x_j = intersection point of integration path with zone j.

The numbers K and the functions L are calculated for all y_k with the same i and compared to the measured data h_k by means of a least-squares criterion

$$\sum_k [h_k(y_k) - (K(y_k) + L(y_k, A_i, B_i))]^2 \stackrel{!}{=} \text{Min}\,. \tag{2.6}$$

Derivation of (2.6) with respect to A_i or to B_i and solving the resulting equation system yields the unknown coefficients and, consequently, the polynomial $P_i(r)$.

Making two additional assumptions at the periphery ($P_0(R_0) = 0$, $P_0'(R_0) = 0$) and one at the centre ($P_{M-1}'(0) = 0$) of the reconstruction region, we can calculate the coefficients of all the M polynomials and hence the complete function $f(r)$.

2.5. Convolution Method for Radial Symmetry

When investigating an asymmetrical distribution $f(r, \varphi)$ by utilizing light transmission, projections $h(l, \Theta)$ must be obtained for different directions Θ. The analytical relationship between them is given by the inverse Radon transformation [12]

$$f(r, \varphi) = \frac{1}{2\pi^2} \int_0^{\pi} \left(\int_{-\infty}^{+\infty} \frac{1}{r\cos(\theta - \varphi) - l} \cdot \frac{\partial h(l, \Theta)}{\partial l}\, \mathrm{d}l \right) \mathrm{d}\Theta, \tag{2.7}$$

which is a general form of (1.2). Several methods, known as *computer tomography*, have been proposed for the numerical handling of this equation and are used successfully, especially in medicine (e.g. [13, 14]). We wanted to use the concepts of such successful methods and tried to adapt them to the case of radial symmetry. As an example we show this simplification for the *convolution method.*

Following [14] it can be shown that for asymmetrical distributions $f(r, \varphi)$, (2.7) can be transformed into

$$f(r, \varphi) = \int_0^{\pi} \left(\int_{-\infty}^{+\infty} h(l, \Theta)\, q_A(r\cos(\Theta - \varphi) - l)\, \mathrm{d}l \right) \mathrm{d}\Theta, \tag{2.8}$$

which is a convolution of the measured data $h(l, \Theta)$ with the convolving function

$$q_A(s) = -2 \cdot \int_0^{A/2} F_A(u) \cdot \sin(2\pi u s)\, \mathrm{d}u\,. \tag{2.9}$$

$F_A(u)$ is a known window function with certain features making possible adequate smoothing of the result. In the case of radial symmetry, (2.8) can be simplified to

$$f(r) = \int_0^{\pi} \left(\int_{-\infty}^{+\infty} h(y)\, q_A(r\cos\Theta - y)\, \mathrm{d}y \right) \mathrm{d}\Theta\,. \tag{2.10}$$

Precalculation of the convolving function $q_A(s)$ at certain points and effective numerical integration of (2.10) make it possible to do these calculations on a PC in a reasonable time ($\ll 1$ min).

2.6. Fourier Method

Many methods of numerical Abel inversion produce results by working gradually from the periphery to the centre, and therefore calculation and measurement errors of the outer parts have an influence on the results in the central region and consequently make these the most uncertain ones. Thus we looked for numerical methods which do not perform the calculations recurrently but in one single step (e.g. [10]).

In an approach very different from those shown above, the unknown radial distribution $f(r)$ is expanded in a series similar to a Fourier series [11]:

$$f(r) = \sum_{n=N_l}^{N_u} A_n f_n(r) \tag{2.11}$$

with unknown amplitudes A_n, where $f_n(r)$ is a set of cosine functions, e.g.

$$f_0(r) = 1\,,$$

$$f_n(r) = 1-(-1)^n \cos\left(n\pi \frac{r}{R}\right). \tag{2.12}$$

Following (1.1), the Abel transform $H(y)$ of (2.11) has the form

$$H(y) = 2 \sum_{n=N_l}^{N_u} A_n \int_y^R f_n(r) \frac{r\,\mathrm{d}r}{\sqrt{r^2-y^2}}. \tag{2.13}$$

The integrals

$$h_n(y) = \int_y^R f_n(r) \frac{r\,\mathrm{d}r}{\sqrt{r^2-y^2}} \tag{2.14}$$

cannot be solved analytically but are calculated numerically in advance and stored in the computer. The amplitudes A_n are still unknown but we can consider that at the N points $y=y_k$, the function $H(y, A_n)$ should approximate the measured values $h(y_k)$. This statement is written as a least-squares criterion

$$\sum_{k=1}^{N} [H(y_k) - h(y_k)]^2 \stackrel{!}{=} \mathrm{Min}\,. \tag{2.15}$$

Insertion of (2.13) followed by analytical differentiation with respect to the unknown amplitudes A_n leads to

$$2 \sum_{n=N_l}^{N_u} \left(A_n \sum_{k=1}^{N} h_n(y_k)\, h_m(y_k) \right) = \sum_{k=1}^{N} h(y_k)\, h_m(y_k), \quad \forall m:\ N_l \le m \le N_u\,. \tag{2.16}$$

Evaluation of this equation system yields A_n, which are inserted into (2.11) and produce the resulting distribution $f(r)$.

This *Fourier method* has some advantages over the numerical processes shown before. On the one hand, it is derivative-free because of the transformation of the whole problem from the r- to the y-space; on the other hand, neither smoothing nor any other kind of pre-treating of the measured data $h(y)$ is necessary. Following this method, the numerical inversion can be used as a noise filter by choosing the lower and upper frequency limits N_l and N_u in (2.16). This can be supported by adaption of the exact form of the model functions $f_n(r)$ to the given physical conditions. Then the upper limit N_u can be chosen low enough for an efficient low-pass filtering because the reconstruction almost entirely depends on the low-frequency components.

3. Comparison by Computer Simulation

3.1. Principle of the Simulation

The study of the influence of typical measurement errors on the results of Abel inversion is important for estimating the quality of the resulting function [4, 15]. Our task was to compare the errors produced by different numerical methods. This was done using a given radial distribution $F(r)$, integrating it analytically or numerically following (1.1) and introducing the errors to be studied. $h(y)$, resulting from these operations is inverted numerically by the methods presented in Sect. 2, thus yielding the function $f(r)$ which can be compared with the given distribution $F(r)$. In this way the reconstruction quality can be controlled easily.

Whenever possible we employed the relative radial course of reconstruction errors for judging the quality of the results:

$$e(r) = \frac{f(r) - F(r)}{F(0)}\,.$$

In all other cases the number

$$p = \frac{\sum |f(r) - F(r)|}{\sum |F(r)|} \tag{3.1}$$

was used as a measure of the reconstruction quality.

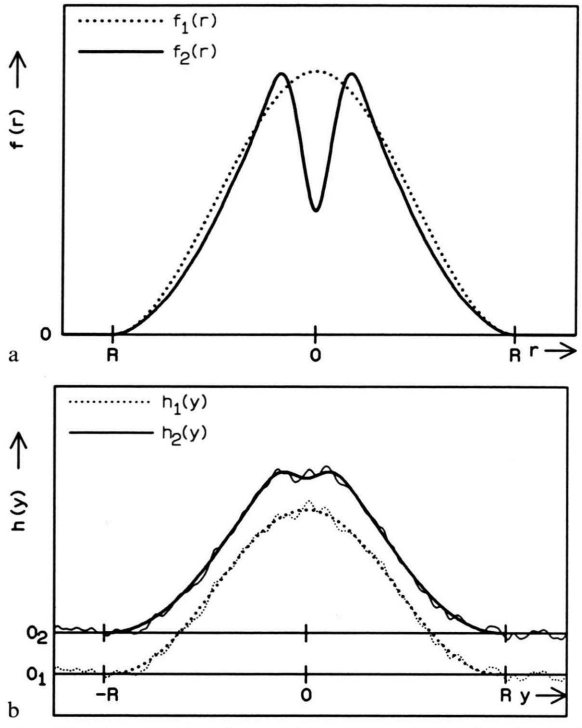

Fig. 3.1. *Two simulated sets of functions:* a) Simulated radial distributions $f(r)$: $f_1(r)$ type of particle density distribution in a cascaded arc, $f_2(r)$ type of particle density distribution in an ICP. b) Abel transforms of the above functions, with and without statistical errors.

We employed polynomials of the third and fourth degree for constructing model distributions $F(r)$. For each of the single polynomials, the forward Abel transformation (1.1) can be performed analytically and an arbitrary number of them with different orders, heights B, and radii R can be put together, which makes it possible to simulate a wide range of distribution types occurring in practice.

For example, the third degree polynomial

$$P_3(r) = B\left(2\frac{r^3}{R^3} - 3\frac{r^2}{R^2} + 1\right) \quad \text{for} \quad r \le R \tag{3.2}$$

can be transformed according to (1.1) to

$$H_3(y) = 2\int_y^R P_3(r)\frac{r}{\sqrt{r^2-y^2}}\,\mathrm{d}r$$

$$= \frac{B}{2}\cdot\left[\left(2-5\frac{y^2}{R^2}\right)\cdot\sqrt{R^2-y^2} + 3\frac{y^4}{R^3}\cdot\ln\left(\frac{R+\sqrt{R^2-y^2}}{y}\right)\right]. \tag{3.3}$$

for $y \le R$.

Examples of functions constructed by composing simple polynomials $P_i(B, R)$ like (3.2) with different i, B

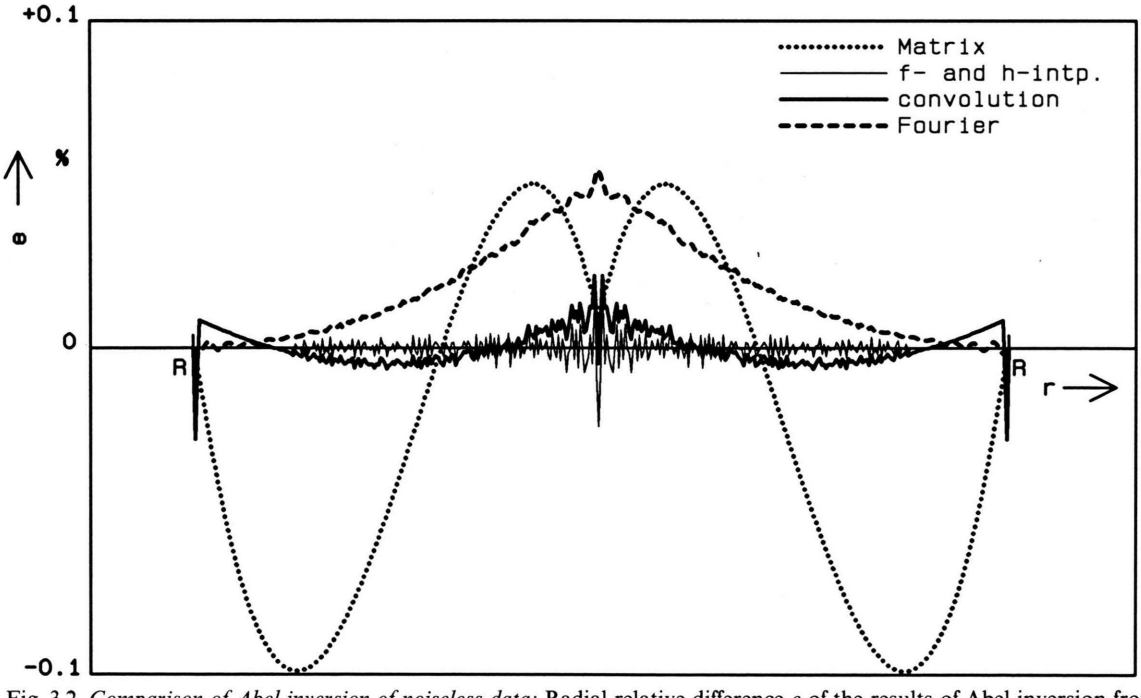

Fig. 3.2. *Comparison of Abel inversion of noiseless data:* Radial relative difference e of the results of Abel inversion from the reference profile (function f_2 in Fig. 3.1 a) for the investigated numerical methods in the case of noiseless projection data $h(y)$.

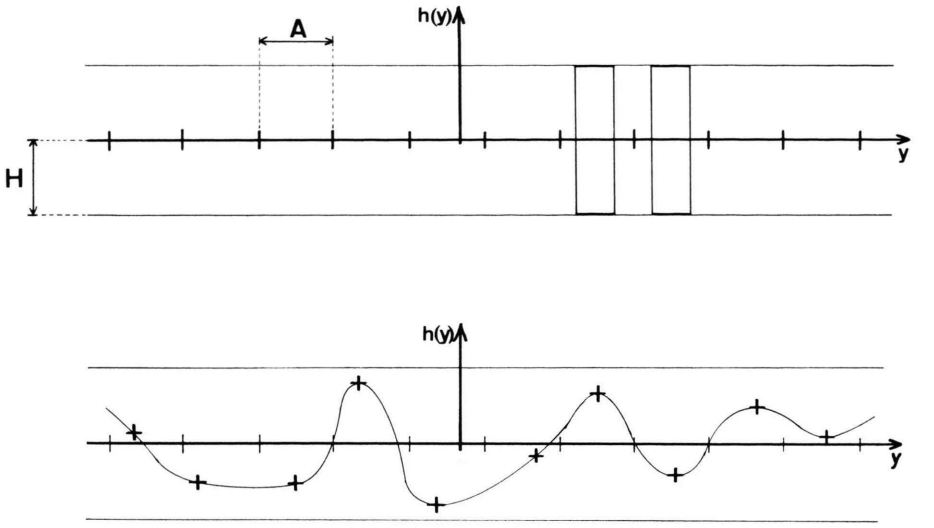

Fig. 3.3. *Simulation of statistical errors:* a) The y-axis is divided into parts of the same size, each being filled with a rectangle (height $2H$ and length $A/2$ freely chosen). b) Points positioned one in each rectangle are connected by third degree polynomials.

and R are shown in Figure 3.1. One of these employed testing functions has a dip in the center because it is known that the reconstruction of such a form is difficult [4].

First we performed the numerical reconstruction of undisturbed simulated projections $h(y)$. An example of the results is given in Figure 3.2. Although differences between the compared numerical methods can be noticed, the order of magnitude of the reconstruction errors is negligible for all of them. Therefore the reconstruction of "perfect data" does not give information on the quality of the different numerical methods but it can be recommended for checking the correct installation of the reconstruction algorithms in the computer.

3.2. Influence of Statistical Noise

Simulating statistical errors should produce data similar to those resulting from real measurements. Thus it is not sufficient to add statistical noise to each pixel separately because in reality the measurement error of one pixel very often is related to that of the neighbour pixels. On the other hand, care has to be taken to prevent some specific property of the error simulation algorithm being studied instead of the errors themselves, but nevertheless this algorithm should be as flexible as possible. According to these requirements we produced statistical errors as follows (see also Figure 3.3):

- The y-axis is divided into parts of length A (the "error length").
- In the centre of each part a rectangle is defined with sides $A/2$ and $2H$ (the "error height").
- In each rectangle one point is positioned with random coordinates.
- All these points are connected by polynomials of the third degree using spline interpolations. The resulting function is added to the "perfect" function $h(y)$.
- By choosing the parameters A and H and adding several different error profiles to one function $h(y)$, it is possible to produce many types of statistical noise.

As a first result of reconstructing noisy data we found that it is not useful to smooth the measured profiles in any way. One never knows whether that only reduces statistical noise or also changes the real information, and what is more, in most cases the latter will happen. The error of the result caused by incorrect smoothing cannot be estimated, not even the order of magnitude. Therefore we recommend that the unchanged measured profiles should be used for the numerical reconstruction.

Doing this for a series of different noisy profiles we saw remarkable differences in the quality of the results using the different numerical methods (see for example Figs. 3.4, 3.5). In detail, the results show that in the case of noisy data the f-interpolation (see Sect. 2.4)

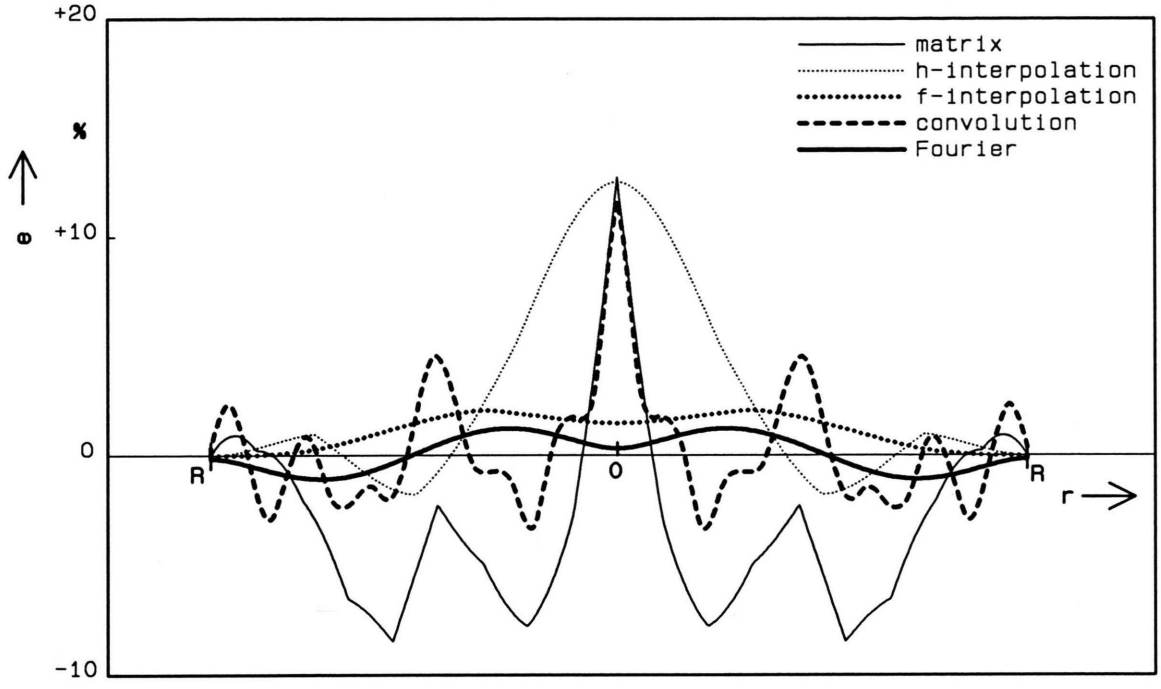

Fig. 3.4. *Comparison of Abel inversion of projection* h_1: Radial relative difference e of the results of Abel inversion from the reference profile for the investigated numerical methods, for f_1 in Figure 3.1.

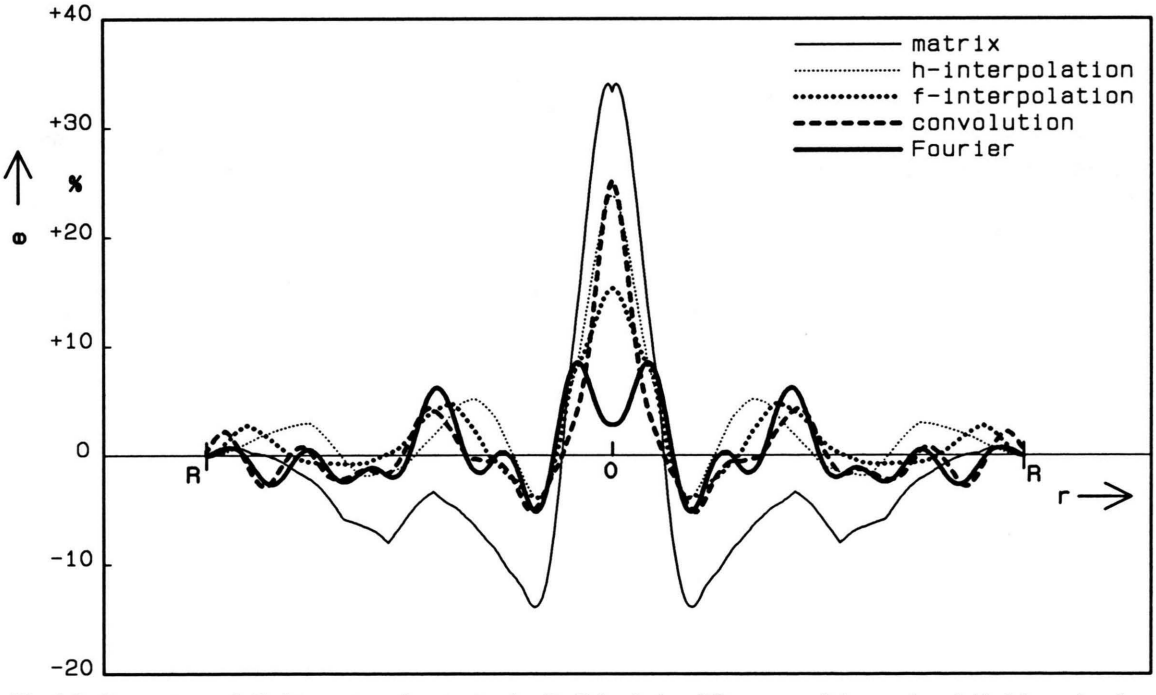

Fig. 3.5. *Comparison of Abel inversion of projection* h_2: Radial relative difference e of the results of Abel inversion from the reference profile for the investigated numerical methods, for f_2 in Figure 3.1.

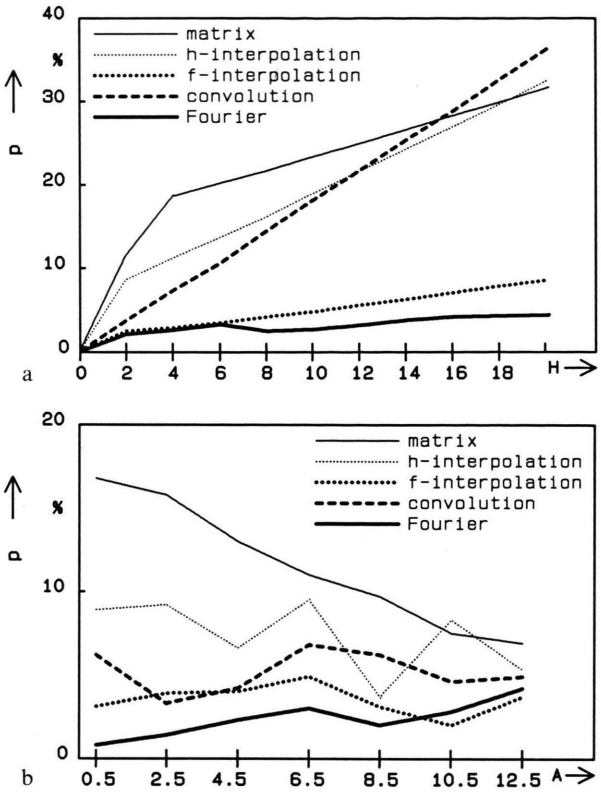

Fig. 3.6. *Dependence of the inversion quality on the error parameters:* a) Reconstruction quality parameter p dependent on error height H. b) p dependent on error length A.

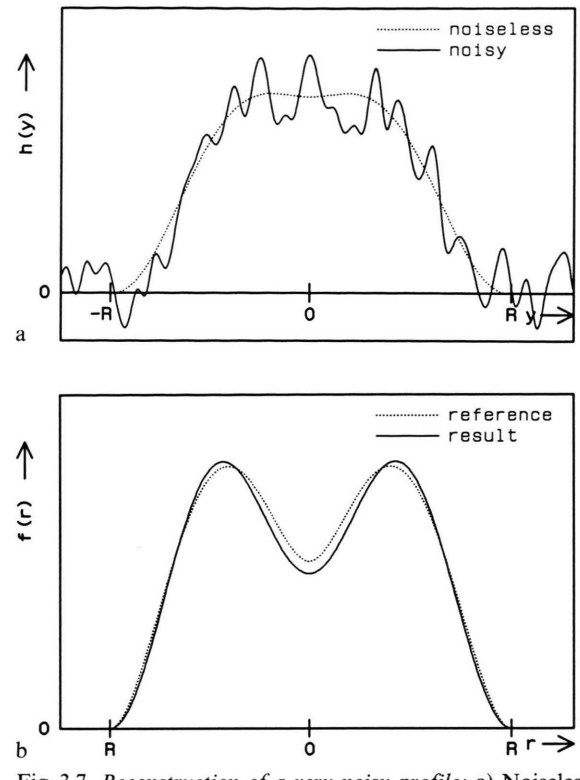

Fig. 3.7. *Reconstruction of a very noisy profile:* a) Noiseless and noisy projection data $h(y)$. b) Reference and result $f(r)$ calculated from the noisy profile shown above with the Fourier method.

and the Fourier method (Sect. 2.6) are superior to the three other methods discussed in Chapt. 2, no matter which profile was reconstructed. Furthermore it can be seen that the more complicated the profile the worse is the reconstruction. In general, there is a large influence of statistical noise on the quality of the results of numerical Abel inversion, especially the centre of an unknown function is often reconstructed badly. So, for example, in Fig. 3.5 errors of up to 35% occur in the center caused by noise typical of practically obtained distributions (Figure 3.1.b).

To give these investigations more generality we varied the error parameters A and H (cf. Figure 3.3). Increasing the error height H (with unchanged A) leads to a roughly linear increase of the error measure p (see Figure 3.6.a). The different slopes obtained using the various methods demonstrate that the Fourier- and the f-interpolation methods are least influenced by statistical noise.

The influence of increasing the error length A (with unchanged H) is shown in Figure 3.6.b. Errors increase with increasing A using the Fourier method, which can be explained by the fact that the number of employed components decrease because the error frequencies become lower. All methods converge towards a common value for the reconstruction error for large A, because the low frequency statistical error converges more and more towards an asymmetrical error (cf. Section 3.5).

In general, even those profiles with huge statistical errors can be reconstructed with satisfactory accuracy (if their error frequency is not too low) by employing the Fourier- or the f-interpolation method (see example in Figure 3.7).

3.3. Position of the Central Point

In practice the exact position of the centre of a measured projection is not known. In this section we report the results of our investigation of the influence of an incorrectly assumed central point on the quality of the reconstruction.

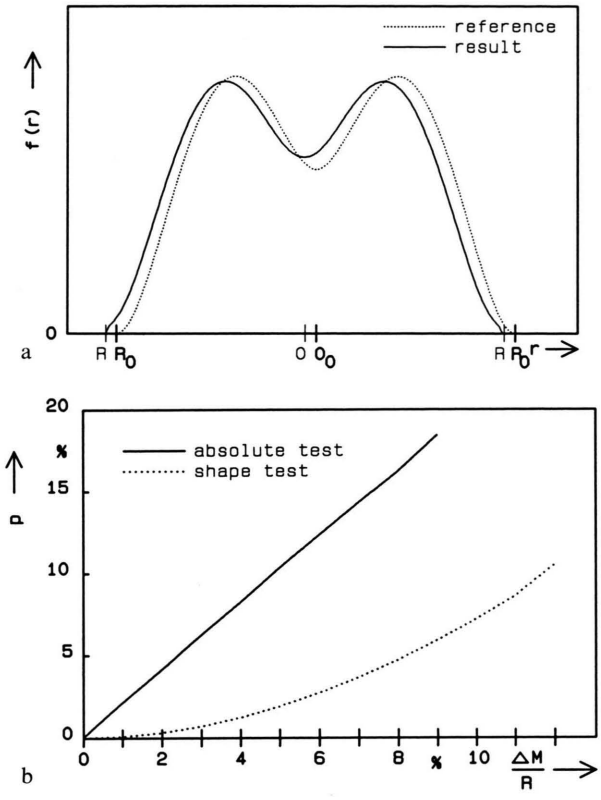

Fig. 3.8. *Effect of an incorrect central point:* a) Result of an inversion made with centre 0 instead of 0_0. b) Dependence of quality parameter p on the position of the central point ($M=0$ is the correct position). The comparison is made with the reference at the correct position (absolute comparison) and with reference shifted to the position 0_0 (shape comparison).

To study this effect separately we used "perfect data" (no statistical noise) for the numerical reconstructions. These functions (real central point 0_0, maximal radius R_0, see Fig. 3.8.a) were reconstructed using the central point 0 at a distance of M from 0_0, while the maximal radius remained unchanged.

As a first result we noticed that all the numerical methods tested gave the same results within a few percents. As shown in Fig. 3.8.a, the form of the profile is not reconstructed too badly, but it is shifted to one side. This can be seen more clearly in Figure 3.8.b. Here the increase of the error measure p is shown as a function of the shift M of the centre on the r-axis. In one case, the result of the reconstruction is compared with the real distribution, demonstrating the absolute reconstruction accuracy. In the other case, the result is compared with the model distribution shifted by the same distance M, which is a measure of the reconstruction of the function shape.

The effects of an unknown centre are much more severe in case of very peaked distributions. Even artificial hollow profiles could be obtained. Therefore it is advantageous to have a method for approximately determining the central point. One method (see e.g. [4]) calculates the y-coordinate of the centre y_c as

$$y_c = \frac{\sum_y (y \cdot h(y))}{\sum_y h(y)}. \tag{3.4}$$

Even this simple formula was able to yield the centre of the distribution with an accuracy better than 2% for all the simulated noisy profiles (1% for profiles with "realistic" noise), which is good enough for a satisfactory reconstruction (cf. Figure 3.8.b).

3.4. Position of the Periphery

If a measurement yields symmetrical but noisy data, the outer limits for the reconstruction procedure cannot be determined unambiguously. Again we studied this effect separately from other error sources. This means here that a model profile with radius R_0 was reconstructed from noiseless data with the same centre but the wrong radius R. Once again all numerical algorithms gave the same results, see for example Fig. 3.9.a: Too narrow limits lead to too small values of the complete function that results. This is easy to explain because the measured function $h(y)$ is set 0 at the limiting points. So the whole function gets too small values if the original limiting points are greater than 0.

More details of the situation are shown in Figure 3.9.b. Too narrow limits result in increasing errors, but too wide limits do not have any obvious effect. This result leads to an easy recipe for avoiding reconstruction errors of this kind: The limits for the reconstruction should always be chosen too wide rather than too narrow.

3.5. Influence of Asymmetries

All the methods for numerical Abel inversion are by definition capable of reconstructing only radially symmetrical functions $f(r)$. On the other hand, one can never be sure in practice whether an arbitrary distribution is really radially symmetrical. What is more,

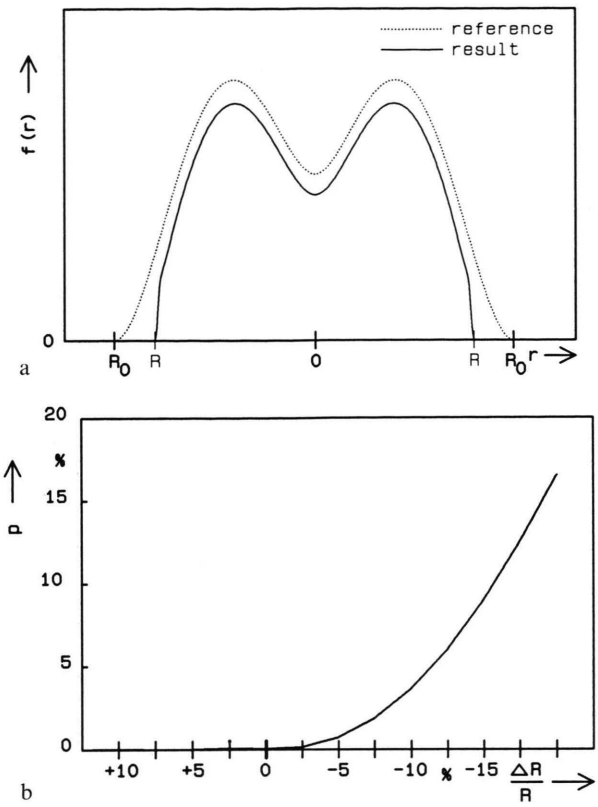

Fig. 3.9. *Effect of incorrect reconstruction limits:* a) Result of an inversion made with maximal radius R instead of R_0. b) Dependence of quality parameter p on the error of the maximal radius R.

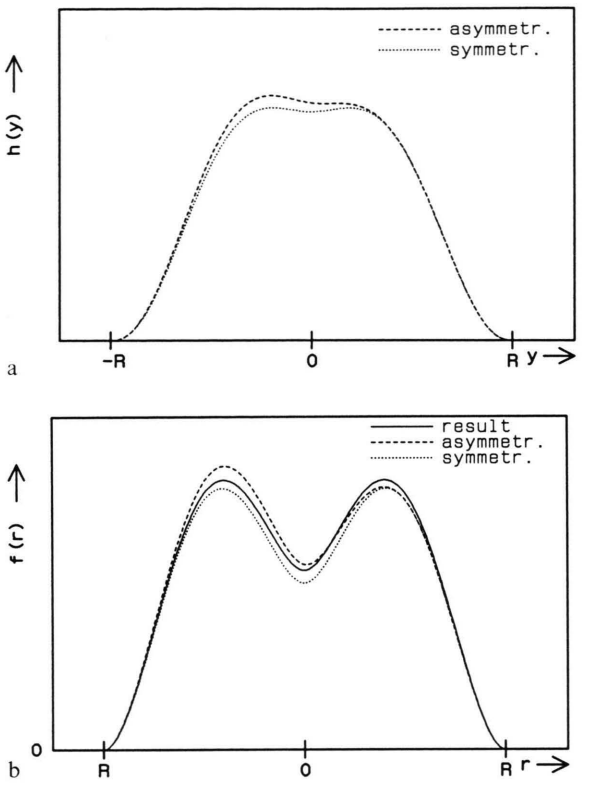

Fig. 3.11. *Reconstruction of an asymmetrical profile:* a) Asymmetrical projection $h(y)$ to be inverted, and its symmetrical part. b) Result of reconstructing the above profile, compared with the asymmetrical reference and its symmetrical part.

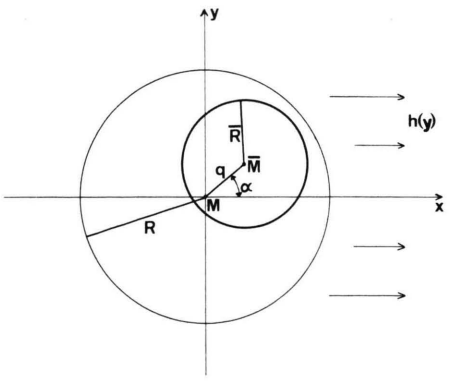

Fig. 3.10. *Simulation of an asymmetric distribution:* One radially symmetrical distribution (centre M, radius R) is superimposed on a second one (centre $\bar{M}$, radius $\bar{R}$). The parameters z (relative height of asymmetrical part), q (distance between the centres) and α (angle of the interconnection line with observation direction) can be varied.

most measured projections $h(y)$ which should be symmetrical with respect to the centre show differences between the two halves. In most cases these asymmetries are the only information available on the geometrical quality of the distribution to be investigated. In this section we try to simulate this situation to find an answer to the question whether the degree of asymmetry of a measured profile can indicate if reconstruction by means of Abel inversion is appropriate.

The simulation of asymmetrical profiles was carried out as indicated in Figure 3.10. Two radially symmetrical distributions were superimposed with different centres. The distribution along the y-axis (i.e. normal to the observation) was used as the reference profile $F(r)$. As in the previous sections the results of the numerical reconstruction were nearly the same for all methods investigated. It can be seen in Fig. 3.11 that the symmetrical part of the distribution is reconstructed correctly, while the asymmetrical part is

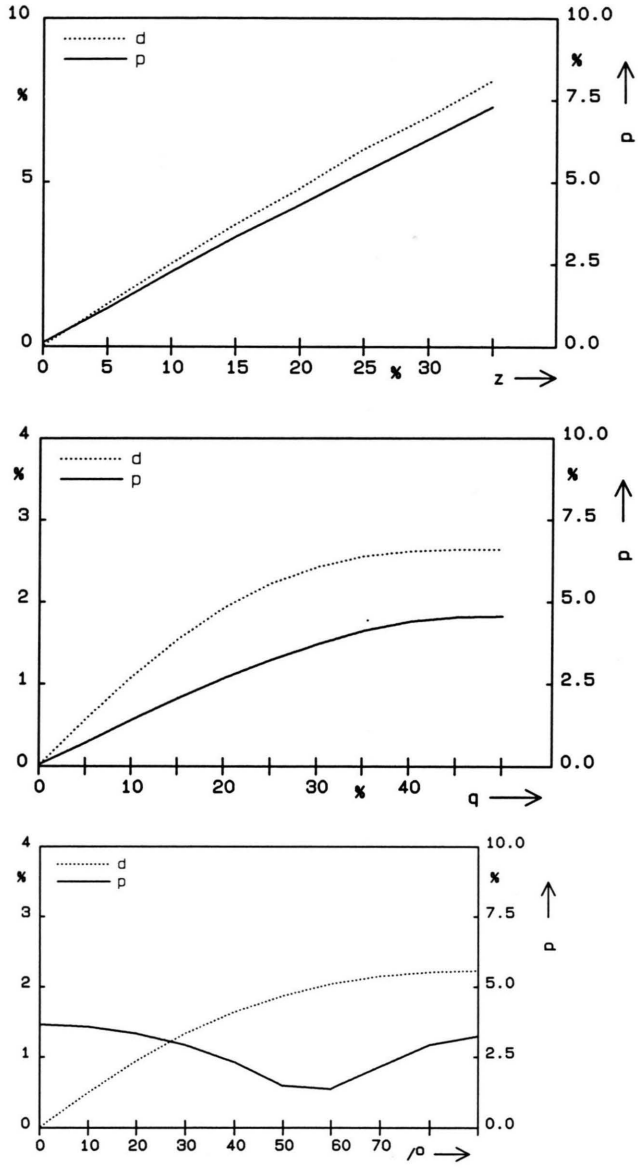

Fig. 3.12. *Effect of varying the asymmetrical parameters:* Parameters d (degree of asymmetry of the projection $h(y)$ to be reconstructed) and p (error measure of the reconstruction result) dependent on the asymmetry parameters (see Fig. 3.10) a) z (relative height of asymmetrical part), b) q (distance between the centres), c) α (angle of the interconnection line with observation direction).

roughly averaged over the whole function. This result is valid for all the different shapes of asymmetrical distributions that we could achieve by varying the parameters q, α, and z (see Figure 3.10).

We see that, although asymmetries by definition cannot be reconstructed, at least they do not introduce nonsense to the result. But this alone is not enough, often one should be able to estimate the accuracy of results and so attempts were made to find limits for the reconstruction errors.

In practice, normally the only information on the shape of an object can be obtained from one measured projection. We define a parameter d as a measure of the degree of asymmetry of the function $h(y)$:

$$d = \sum_{y=0}^{y_m} \left| \frac{h(y) - h(2y_m - y)}{h(y)} \right| . \tag{3.5}$$

with y_m = central point.

Our objective was to investigate whether or not there is a correlation between this projection asymmetry d and the reconstruction error p (cf. (3.1)). To do this we varied each of the three free parameters of the asymmetrical simulation separately (see Fig. 3.10), holding the others constant.

Figure 3.12 represents the results of these calculations. In Fig. 3.12.a (dependence of the reconstruction quality on the relative height z) the correlation is excellent, in Fig. 3.12.b (dependence on the distance q between the centres of the symmetrical and the asymmetrical parts of the simulated distribution) it is good. In Fig. 3.12.c (dependence on the angle α of the asymmetrical part), however, we must note that the correlation between d and p is very poor. It is easy to understand that for $\alpha = 0$ no sign for asymmetry can be found in the measured data, but it is clear that the result of the numerical Abel inversion is poor.

This last result makes it impossible to find a general estimate for the probable reconstruction error to be expected. The only information we can take from calculating the parameter d is a *lower limit* for p:

$$p \geq d/2 . \tag{3.6}$$

This can at least exclude profiles with a too high degree of asymmetry from Abel inversion reconstructions. In this case or in the case of uncertain geometry we refer to tomographic methods or at least to the measurement of a second projection orthogonal to the first in order to provide more information about the shape of the object.

3.6. Combination of Different Error Types

In real measurements all the error types treated individually above occur in combination. For studying this real situation we produced profiles with all the errors investigated above superimposed.

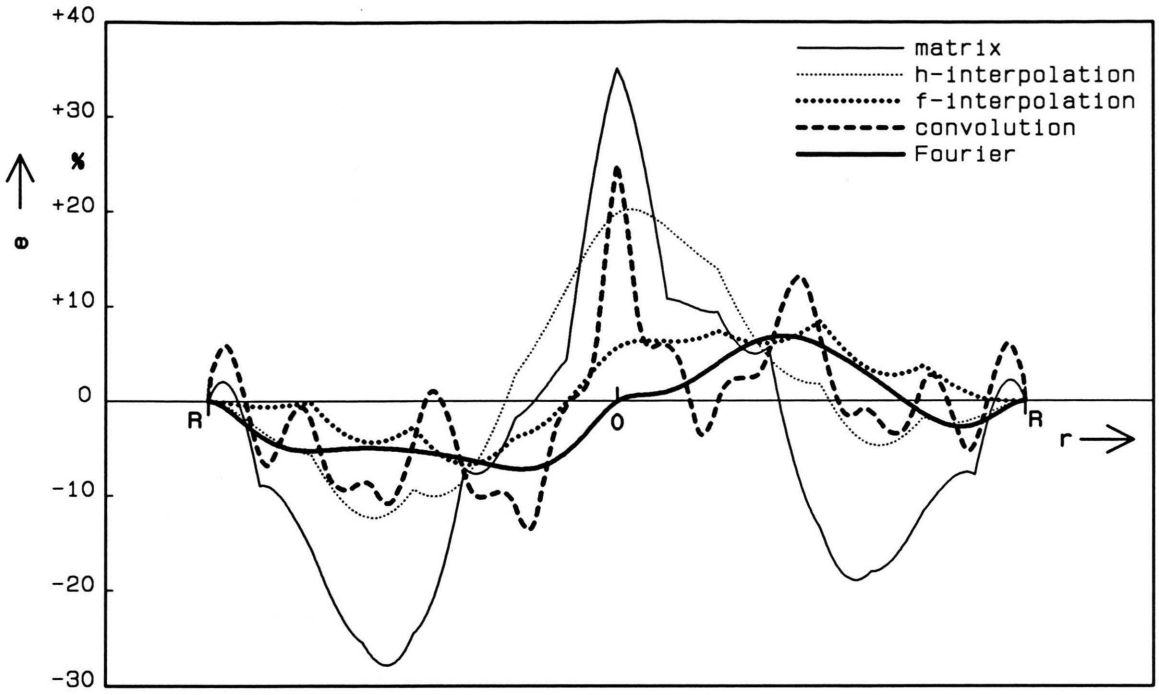

Fig. 3.13. *Comparison of Abel inversion of a profile with both statistical and systematical errors:* Radial relative difference e of the results of Abel inversion from the reference profile for the numerical methods investigated. The projection to be inverted is superimposed with statistical and asymmetrical errors (cf. Figs. 3.4, 3.11).

The results show that the effect of statistical errors is roughly added to the effect of any systematical error, see for example Figure 3.13. Since the *f*-interpolation and the Fourier method have proved to be best in minimizing the effects of statistical errors, and since there was no other significant difference of the methods to be compared, we recommend one of these two methods for numerical reconstructions.

Errors arising from uncertainty in the limits of the reconstruction region can always be minimized by choosing the limits too wide rather than too narrow, no matter if there are also other error types.

One problem still remaining is the calculation of the position of the central point in the presence of asymmetries. It can be shown by simulation that in cases of promising profiles (cf. Fig. 3.11), the position of the central point can be calculated with the proposed formula (3.4) with an error small enough ($\Delta M/R \leq 2\%$) not to significantly disturb the result (see Figure 3.8.b).

All these results obtained by extensive computer simulations can be used to minimize and estimate reconstruction errors of real data.

4. Comparison with Experimental Data

4.1. Description of the Experiment

In the last chapter we developed recipes for minimizing errors of numerical Abel inversion by means of computer simulation. To demonstrate the usefulness of these concepts in practice we had to perform an experiment allowing the determination of some radially symmetrical quantity $f(r)$ (cf. Fig. 1.1) in two ways. On the one hand, a projection $h(y)$ should be measured and inverted numerically. On the other hand, the quantity $f(r)$ should be measured in a different, independent way, if possible directly.

We employed an experiment described in [16] with a convective stream of hot air (produced by a chimneylike device, maximum temperature ≈ 80 °C) as the object of which the temperature should be measured. Air flows into an oven from the bottom, is warmed up by an electronically stabilized ohmic heating and leaves the device through a circular opening at the top. Exactly in the centre of this opening, cold air can be blown out to produce more complicated temperature profiles. It was shown that the stabilized heating and

the water cooling of the cover of the device resulted in stationary conditions of the temperature distribution for many hours (at maximum temperature, $\Delta T \approx 0.5$ °C at most).

The temperature of the hot air stream was measured in a plane 7.5 mm above the outlet from the heating device in two different ways. A dot-like NTC sensor (NTC for negative temperature coefficient) could be moved through the test zone fixed on the short arm of a pantograph, the long arm of which was used for exact positioning. In this way the temperature could be measured with a spatial resolution of 1.7 mm in both x- and y-direction.

Apart from this we made a holographic interferogram of the object [17, 16], thus determining the phase shift of light introduced by the hot air flow. A hologram of the object is taken before switching it on and the undisturbed wavefronts coming from the object are stored this way. When the air stream has reached stable conditions this hologram is reconstructed and the beam carrying the undisturbed wave fronts interferes with the actual object beam. Interference fringes result from the phase shift introduced to the actual object beam by the changes of the refractive index in the test zone. For improving the accuracy of evaluation we used optical heterodyning [18, 19, 16] by superimposing equidistant carrier fringes onto the interference pattern, achieved by slightly tilting one mirror in the optical arrangement between taking the hologram and recording the interferogram.

The resulting interferogram was evaluated using Fourier transformation, frequency filtering around the carrier frequency and inverse transformation [18, 16]. The resulting phase shift $h(y)$ is the projection which can be reconstructed by means of numerical Abel inversion, thus producing a differential phase shift $f(r)$ proportional to the difference of the index of refraction Δn between heated and normal state at the radius r,

$$f(r) = \Delta n(r) \frac{2\pi}{\lambda} b\,, \tag{4.1}$$

where λ is the wavelength of the laser light and b is a scaling factor. The relationship between the refractive index n and the temperature T is given by [20]

$$(n(r)-1) = (n_0-1)\frac{1+\alpha t_0}{1+\alpha T(r)}\frac{p}{p_0} - \left(\beta - \frac{\gamma}{\lambda_0^2}\right) p_d\,, \tag{4.2}$$

where t_0, p_0, n_0 are the standard values for temperature, pressure and refractive index, α, β, γ are con-

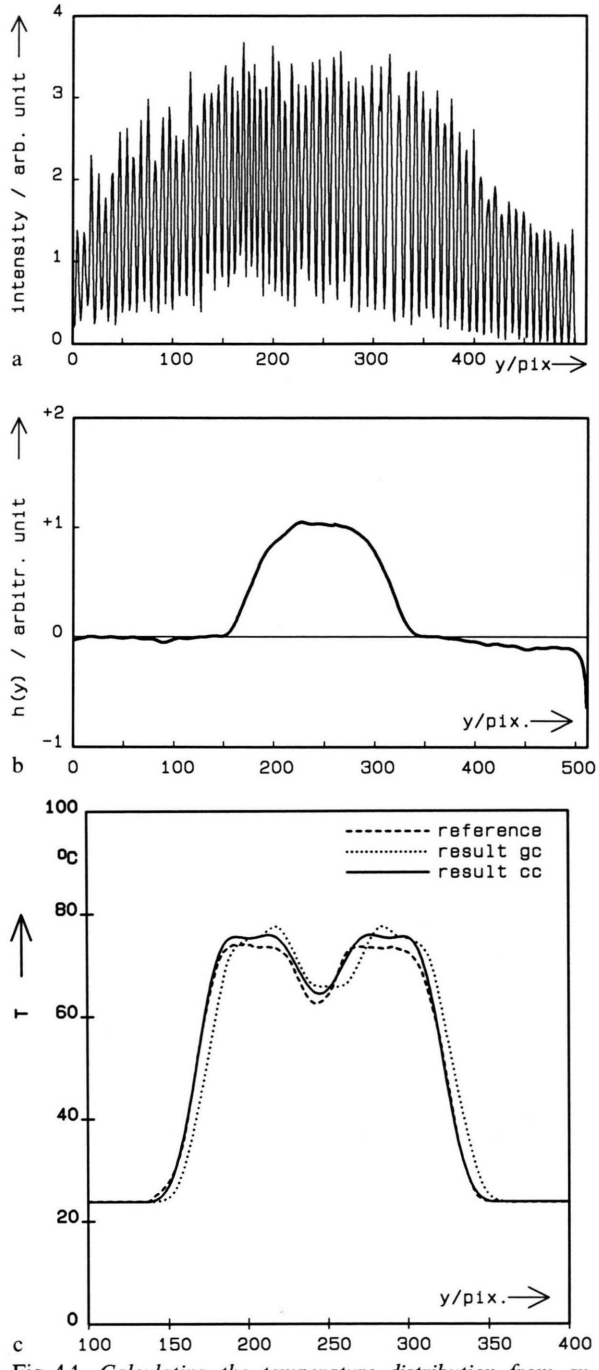

Fig. 4.1. *Calculating the temperature distribution from an interferogram:* a) Intensity distribution of one line of a heterodyne holographic interferogram. b) Phase distribution of a) after elimination of the constant incline caused by the carrier frequency. This is the projection $h(y)$ to be inverted numerically. c) Radial temperature distribution in the test zone. Reference (measured independently with NTC-sensor) and results calculated from b) with geometrical (gc) and calculated (cc) centre, respectively.

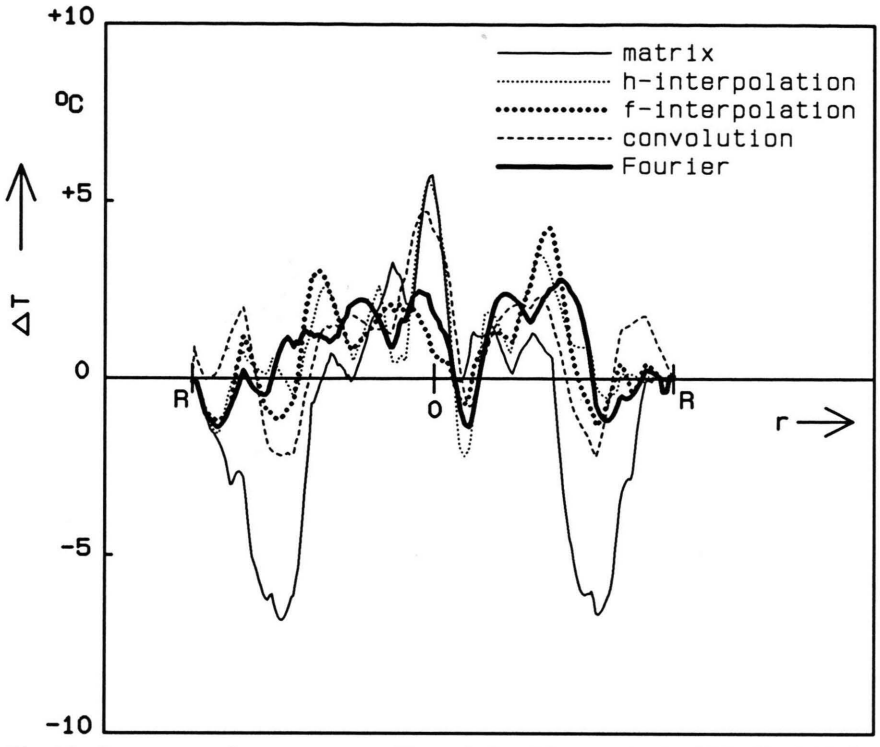

Fig. 4.2. *Comparison of temperature profiles, calculated from projection $h(y)$, Fig. 4.1.b:* Radial relative difference ΔT of the temperatures obtained by Abel inversion from the profile measured independently for the numerical methods investigated.

stants, p, p_d are the air pressure and the partial pressure of water, respectively.

So the evaluation of the holographic interferograms leads to the calculation of the local temperature in the convective air stream which can be compared with the temperature of the independent NTC-measurement.

4.2. Results of the Experimental Comparison

The process of achieving the temperature distribution will now be described in detail with one example.

- A holographic interferogram was taken and its intensity profile was digitized exactly in the height of the test zone (see Figure 4.1.a).
- From this profile, the phase shift $h(y)$ introduced by the object was determined (for description see above, for result see Figure 4.1.b).
- From the projection $h(y)$ the radial temperature distribution was calculated using numerical Abel inversion and (4.1), (4.2).
- The numerical Abel inversion was carried out in two different ways. (i) The geometrical centre of the orifice of the oven was used as central point of the reconstructing algorithms; (ii) the centre was calculated using (3.4). Fig. 4.1.c shows that in this case the concepts developed in Chapt. 3 are more trustworthy than extra information on the object (geometry). Here the result using the geometrical centre has a reconstruction error $p=7.8\%$, while that using the calculated centre (difference $M\approx 5\%$) has $p=1.3\%$ (cf. Figure 3.8.b).
- A comparison of all the numerical methods that we employed (see Fig. 4.2) proves that the temperature profile is calculated to be slightly high using all methods, which according to Chapt. 3 indicates systematic errors. The asymmetry measure d (see (3.5)) of the projection $h(y)$ has the value $d=2.0\%$, thus indicating that $p \geq 1.0\%$, which is in accordance with reality ($p = 1.3\%$).
- The maximal deviation of $\Delta T = 2.5\,^{\circ}\mathrm{C}$ (Fourier method) is a sign of the efficiency of both the experimental and the numerical methods used.

We think it is instructive to show a second example giving a view on the limits of all numerical methods of Abel inversion. The phase distribution $h(y)$ obtained by evaluating an interferogram and shown in Fig. 4.3.a

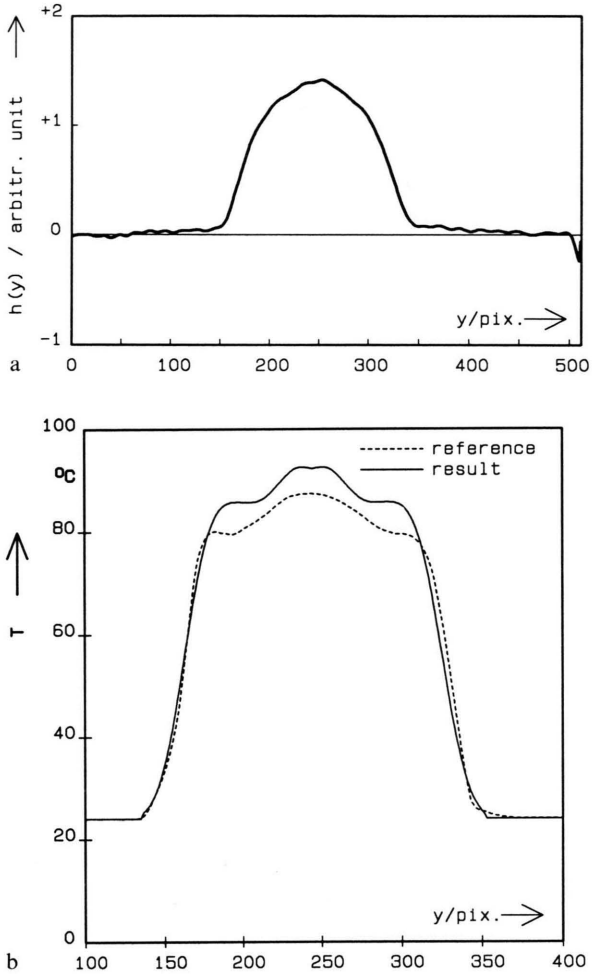

Fig. 4.3. *Calculating an asymmetrical temperature distribution from an interferogram:* a) Phase distribution in one line of an interferogram. This projection to be inverted does not show too much asymmetry. b) Radial temperature distribution in the test zone. Reference (measured independently with NTC-sensor) and result of numerical inversion. The difference between the two profiles can be explained by asymmetries, the error of the reconstruction result cannot be minimized or even estimated in practice.

has an asymmetry coefficient $d = 1.2\%$, indicating that the error measure p should be above 0.6%. Nevertheless, numerical reconstruction, calculation of the temperature profile, and comparison with the independently measured profile yields $p = 5.6\%$ (Figure 4.3.b). We can explain this result because the reference measurement was made within the complete plane and proved that the distribution to be measured had elliptical geometry (axis ratio 11:10) with the main axis in the direction of observation. In reality, when no reference measurements are made, it is impossible to discover this departure from radial symmetry, and even estimating the resulting errors is impossible.

5. Conclusion, Results

This work is devoted to a comparison of five different numerical methods for Abel inversion on the one hand, and to an analysis of error propagation when performing them on the other hand. We arrive at the following results and recipes concerning the errors on the measured data:

- The five methods employed differ only in their behaviour towards statistical measurement errors. Systematic errors have nearly the same influence on the result using all methods.
- Measured profiles should never be smoothed but be inverted unchanged as they have been measured.
- The centre of a distribution should be calculated from the measured profile, even if it is known from other information (e.g. geometry).
- Errors caused by unknown reconstruction limits can be minimized by choosing the limits rather too wide than too narrow.
- Errors arising from asymmetries can only roughly be estimated. In the case of too much uncertainty, tomographic methods should be employed.

The comparison of different numerical inversion algorithms led us to the following results:

- The results concerning statistical errors of the matrix method are bad, so we advise against using it.
- The employed *h*-interpolation method is not suited for profiles with "many" data points (here $N \approx 500$) and should not be used in such cases.
- The adapted method from computer tomography (convolution method) gives worse results than algorithms for the special case of radial symmetry, and it has longer calculation times. Therefore it is not efficient here.
- The method called *f*-interpolation shows good results and is very efficiently programmable, therefore it can be recommended for practice.
- The Fourier method shows the best results because of its implicit employment as a low-pass filter.

In practice we recommend first to create experimentally radial symmetry, then to reduce systematical errors using the methods proposed here, and last to perform the numerical Abel inversion using the Fourier method or *f*-interpolation.

[1] N. H. Abel, Euvres Complètes, Oslo 1881: Vol. 1, 11 (1823); 97 (1826).
[2] J. Friedrich, Ann. Physik, 7. Folge, **3,** 327 (1959).
[3] W. Frie, Ann. Physik, 7. Folge, **10,** 332 (1963).
[4] M. Kock and J. Richter, Ann. Physik, 7. Folge, **24,** 30 (1969).
[5] H. Hörmann, Z. Physik **97,** 539 (1935).
[6] B. Einarsson, Numerical solution of Abel's integral equation with spline functions, Försvarets Forskningsanstalt, FOR 2 Rapport 1 C2455-11 (25) (1971).
[7] S. Ugniewski, Zastowania Matematyki **16,** 91 (1977).
[8] T. L. Bock, Ann. Physik, 7. Folge, **34,** 335 (1977).
[9] P. Andanson, B. Cheminat, and A. M. Halbique, J. Phys. D: Appl. Phys. **11,** 209 (1978).
[10] T. Shimizu and T. Horigome, Contrib. Plasma Phys. **29,** 307 (1989).
[11] G. Pretzler, Z. Naturforsch. **46a,** 639 (1991).
[12] J. Radon, Über die Bestimmung von Funktionen durch ihre Integralwerte längs gewisser Mannigfaltigkeiten, Ber. Verh. Saechs. Akad. Wiss. Leipzig, Math. Phys. Kl. **69,** 292 (1917).
[13] A. M. Cormack, J. Appl. Phys. **34,** 2722 (1963).
[14] G. T. Herman, Image Reconstruction from Projections, Academic Press, New York 1980.
[15] J.-P. Lanquart, J. Computational Physics **47,** 434 (1982).
[16] D. Vukičević, H. Jäger, T. Neger, H. Philipp, and J. Woisetschläger, Appl. Opt. **28,** 1508 (1989).
[17] Yu. I. Ostrovsky, M. M. Butusov, and G. V. Ostrovskaya, Interferometry by Holography, Springer-Verlag, Berlin 1980.
[18] M. Takeda, H. Ina, and S. Kobayashi, J. Opt. Soc. Amer. **72,** 156 (1981).
[19] A. Džubur and D. Vukičević, Appl. Opt. **23,** 1474 (1984).
[20] F. Kohlrausch, Praktische Physik, Bd. 1–3, 23. Aufl., Teubner, Stuttgart 1985.